

Here Be Dragons: Bimodal posteriors arise from numerical integration error in longitudinal models

Tess O'Brien, Matt Moores, David Warton, & Daniel Falster

February 18, 2025

Abstract

Longitudinal models with dynamics governed by differential equations may require numerical integration alongside parameter estimation. We have identified a situation where the numerical integration introduces error in such a way that it becomes a novel source of non-uniqueness in estimation. We obtain two very different sets of parameters, one of which is a good estimate of the true values and the other a very poor one. The two estimates have forward numerical projections statistically indistinguishable from each other because of numerical error. In such cases, the posterior distribution for parameters is bimodal, with a dominant mode closer to the true parameter value, and a second cluster around the errant value. We demonstrate that bimodality exists both theoretically and empirically for an affine first order differential equation, that a simulation workflow can test for evidence of the issue more generally, and that Markov Chain Monte Carlo sampling with a suitable solution can avoid bimodality. The issue of bimodal posteriors arising from numerical error has consequences for Bayesian inverse methods that rely on numerical integration more broadly.

1 Introduction

The use of numerical integration in methods for estimating differential equation parameters from observations introduces a source of error (Butcher, 2016) that is distinct from other processes such as measurement error (Agapiou et al., 2014). In the Bayesian inverse method literature, the effect of numerical error on the posterior distribution is under-explored and we wish to present both a case study on problems and a means for investigating them under similar circumstances.

We have identified a specific pathology arising from numerical error: bimodality of posterior parameter distributions for affine first order ODEs. We first observed bimodality arising from numerical methods during the development of the R package `hmde` (O'Brien et al., 2025). The bimodality leads to independent Markov Chain Monte Carlo (MCMC) chains converging to very different, but very specific, parameter combinations: one which was a good estimate of the true values (ie. parameters known from simulation), and a separate very bad estimate. For the erroneous combination, *under the chosen numerical method and step size*, forward projection produces estimated $Y(t_j)$ over time that are statistically indistinguishable from the ones produced by the

correct parameters, due to numerical error. The posterior is, after all, conditioned on the numerical method used in the model, not the true solution to the integral. As our case study arose from ecological literature, we are thinking about growth functions for DEs, and growth parameters as what is being estimated. The language we use will reflect that background but the situation is more general.

Non-identifiability is a general statistical concept for a situation where multiple estimate values have an indistinguishable relationship to data (Rothenberg, 1971). The form of non-identifiability we are dealing with is different to cases described in the literature. For example Gelfand and Sahu (1999) discusses situations where the set of observations is small relative to the parameter space such as can arise in generalised linear mixed effects models. Auger-Méthé et al. (2016) addresses large measurement error as a potential source, and Cockayne et al. (2019) discusses a situation where the posterior distribution is bimodal because there are two true solutions to the underlying function. Numerical error as a source of estimation problems is rarely addressed in the existing literature. The only mentions we found were Agapiou et al. (2014) looking at convergence for MCMC at different levels of discretisation, Cotter et al. (2010) where the step size of an Euler method was found to bias estimates. Posterior multimodality arising from numerical methods appears to be completely novel.

When bimodality arises from numerical error, stability of the integration method matters for potentially a very large region of the parameter space – far beyond true or even plausible parameter combinations – the boundaries of which are probably unknown when first going in. The numerical methods we use (Runge-Kutta 4 and 4-5 order) are extremely common (*e.g.* Falster et al., 2017), and numerically better than other commonly used methods such as Euler (implemented in Cotter et al., 2010 and Iida et al., 2014). We have identified that the problem arises theoretically, and is empirically observable, for an affine first-order ordinary differential equation with negative slope, such as the von Bertalanffy (Von Bertalanffy, 1938) model where we first observed it, and which is our central example in a re-parameterised form. Affine ODEs are common, and the RK4 method is typically considered reliable for short step sizes (Butcher, 2016). To find a situation where the combination of the two produced a novel pathology was unexpected. While the affine model has an analytic solution which can be implemented, that is not always the case.

After demonstrating the mathematical presence of multiple solutions to parameter estimation, we present a simulation workflow that allows the user to test the parameter space for multimodal pathologies before embarking on large-scale analysis. Our testing starts with MCMC estimation, with different numerical methods, priors, and parameter combinations which still produce bimodal posteriors. The problem persists for deterministic estimation methods that use gradient ascent to maximise the likelihood, such as the L-BFGS algorithm (Nocedal and Wright, 2006). We report the results of experiments to demonstrate how the problem appears in practice, and investigate whether common approaches to dealing with such issues work. We have another function of interest – the extremely non-linear Canham function (Canham et al., 2004) – so we use the simulation workflow to test whether we find evidence of bimodal posteriors for parameters in that case as well.

Our use of simulation is distinct from the simulation-based calibration method (Talts et al., 2020;

Modrák et al., 2023) which uses data simulated from the chosen prior to test the consistency of the posterior with rank statistics. We are doing a predominantly qualitative rather than quantitative analysis testing for evidence of the existence of posterior bimodality arising from numerical error, and use simulated data that does not come from the chosen priors. We consider this a reasonable approach because our intent is to demonstrate the existence and mechanism by which numerical bimodality arises, we already have a fix for our use-case in the affine ODE’s analytic solution. In the spirit of Gelman et al. (2020), deliberately breaking a model can be informative, and we aim to present a generally applicable workflow using simulation for testing whether an intended model is susceptible to these novel problems.

1.1 Theory

We will demonstrate the bimodal posterior estimate behaviour for dynamics based on the affine first-order ordinary differential equation (ODE)

$$f(Y(t), \beta_0, \beta_1) = \beta_0 - \beta_1 Y(t), \tag{1}$$

under the longitudinal model

$$Y(t_{j+1}) = Y(t_j) + \int_{t_j}^{t_{j+1}} f(Y(t), \beta_0, \beta_1) dt. \tag{2}$$

Equation (1) is considered a particularly pathological example for numerical methods (Butcher, 2016) as it is unbounded above and below, and the negative slope in particular means that negative growth increments can arise from the numerics even if the underlying system is strictly positive. The move from continuous time in the analytic solution to discrete time in the numerical one can result in estimates of $Y(t)$ oscillating around the asymptotic size as the calculated gradient overshoots 0 then is pulled back by being a negative value as seen in Figure 1. Equation (1) serves as an ideal example of the bimodal posterior because of the known pathologies, it is simple with two parameters, and has an analytic solution which allows us to easily access true values for $Y(t)$ without introducing compounding numerical error. The analytic solution is

$$Y(t) = \frac{\beta_0}{\beta_1} + \left(Y(0) - \frac{\beta_0}{\beta_1} \right) \exp(-\beta_1 t), \tag{3}$$

which asymptotes to

$$\lim_{t \rightarrow \infty} Y(t) = \beta_0 / \beta_1.$$

We have chosen initial conditions $0 < Y(0) = 1 < \frac{\beta_0}{\beta_1}$, but the asymptote happens regardless as larger sizes with negative slope decrease, and negative sizes with positive slope increase. Equation (3) thus gives a mathematical model that is defined for regions that may not correspond to realistic behaviour in the system being modeled. For example, if Y represents size as in our ecological inspiration, $Y(t) < 0$ is physically impossible.

In the posterior bimodality there is a form of non-identifiability (i.e. non-uniqueness of parameters) that arises from numerical errors in a model based on Equation (2). This non-identifiability

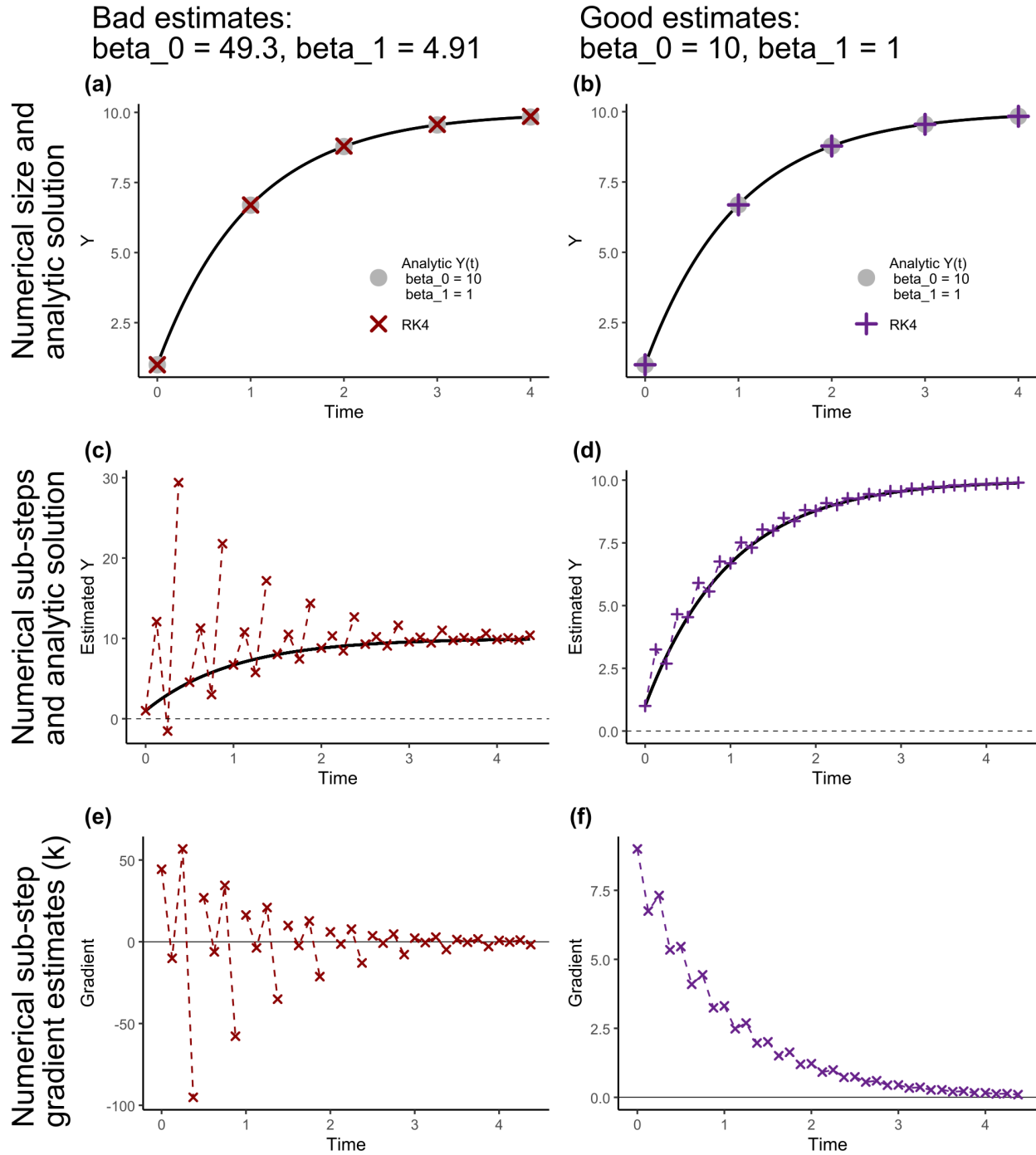


Figure 1: Behaviour of numerical solutions at erroneous and true parameter locations showing considerable instability at the erroneous point. The true $Y(t_j)$ values are those of the analytic solution with $\beta_0 = 10$ and $\beta_1 = 1$ that the model attempts to estimate. (a) and (b) compare the estimated sizes for integer times between 0 and 4 to the analytic solution to show both the good and bad parameters give numerical values very close to the analytic ones. In (c) and (d) we see the sub-steps as well, which are connected up based on the numerical step they come from. The bad parameter estimates demonstrate considerable instability and even a negative value. (e) and (f) give the gradients at the numerical sub-steps and show why the estimated sizes are so unstable for the bad estimate as the gradient oscillates about 0.

is separate to other sources of such problems (Latz, 2023), and currently under-explored in the literature because as far as we can tell it has not been observed before. In this demonstration we use a Runge-Kutta 4th order numerical method (Butcher, 2016) with different step sizes to show that even ‘small’ step sizes (small enough to have good behaviour at the true parameters) can give problems. A step size in this context is the length of a single iteration of the numerical integral, and is at most the time between observations: $t_{j+1} - t_j$. As we are using synthetic data, we have observations 1 unit of time apart, and take our step sizes to be 0.5, 0.25, and 0.125 which divide 1 evenly.

We stress that ‘statistically indistinguishable’ $\hat{Y}(t)$ values in this context means within statistical error of each other, they may not be convergent from an analytic perspective. The statistical equivalence gets involved because we have error and a certain level of resolution in measurement processes. That is, we assume data consists of finite observations of the form y_j at time t_j that look like

$$y_j = Y(t_j) + \text{error},$$

and have some finite level of precision. The numerical method may produce estimated values $\hat{Y}(t_j)$ that differ from the true $Y(t_j)$ by some amount that is much smaller than the level of precision or observation error for the different parameter combinations, but due to the imprecision of the measurement process the likelihood cannot meaningfully distinguish such $Y(t_j)$ and $\hat{Y}(t_j)$. In the Bayesian inverse method literature, this is an issue of practical identifiability, where a finite number of observations combined with measurement error complicate access to the true parameters (Latz, 2023).

For this demonstration we will use added error of $\mathcal{N}(0, 0.1)$ and rounding to produce simulated data with measurement precision of 0.1, analogous to 1 mm measurement precision and standard deviation on observations in centimetres. The scale of measurement is chosen because the method in O’Brien et al. (2024) and O’Brien et al. (2025) was developed for use in ecological size data where such structure shows up (Condit, 1998). We want to demonstrate a realistic measurement process, but the bad numerical behaviour occurs even with a high level of precision, and much smaller error as the underlying cause is mathematical.

We are attempting to estimate the parameters β_0 and β_1 from observations y_j , which is based on estimating \hat{Y}_j given the prior distribution

$$y_j \sim \mathcal{N}(\hat{Y}_j, 0.1)$$

and the longitudinal model in Equation (2), which encodes the auto-correlation in the longitudinal data. For this demonstration we are looking at a single simulated individual. To make fitting the model easier we apply a translation by the mean observed size \bar{y} , which produces the implemented DE

$$f(Y(t), \beta_c, \beta_1, \bar{y}) = \beta_c - \beta_1(Y(t) - \bar{y}).$$

The translation does not mathematically change the behaviour of $Y(t)$. We extract estimates for

β_0 by back-transforming β_c as by definition

$$\beta_0 = \beta_c + \beta_1 \bar{y},$$

so the output estimates are consistent with Equation (1). We have default prior distributions for the parameters which are

$$0 < \beta_1 \sim \log \mathcal{N}(0, 2), \quad \beta_c \sim \mathcal{N}(1, 2),$$

where the mean and standard deviation for β_1 are for the underlying log-transformed normal distribution. The minimal hierarchical set-up is based on the single individual von Bertalanffy structure from O'Brien et al. (2025), but with a number chosen for the error standard deviation instead of fitting an error parameter.

1.2 What's going on inside the numerical method?

Before we give a thorough statistical analysis of the posteriors, we demonstrate what the underlying problem is. In the following we compare the numerical behaviour of the Runge-Kutta 4th (RK4) order algorithm with step size 0.5 at the true parameter values we are working with for this demonstration ($\beta_0 = 10$ and $\beta_1 = 1$), and the behaviour of the same algorithm at the 'bad' estimate point we found for that method and step size: $\hat{\beta}_0 = 49.3$ and $\hat{\beta}_1 = 4.91$.

For those unfamiliar, the RK4 method uses a weighted average of gradients across an interval to predict the next size (Butcher, 2016). Given an initial size $Y(t_j)$, fixed parameter values β_0 and β_1 , and a numerical step size $h = t_{j+1} - t_j$, we estimate

$$\hat{Y}(t_j + h) = Y(t_j) + \frac{h}{6}(k_1 + 2k_2 + 2k_3 + k_4), \quad (4)$$

where the k values are estimates of the gradient based on the DE

$$f(Y(t), t, \beta_0, \beta_1) = \frac{dY}{dt},$$

with formulas calculated iteratively

$$\begin{aligned} k_1 &= f(Y(t_j), t_j, \beta_0, \beta_1), \\ k_2 &= f(Y(t_j) + k_1 h/2, t_j + h/2, \beta_0, \beta_1), \\ k_3 &= f(Y(t_j) + k_2 h/2, t_j + h/2, \beta_0, \beta_1), \\ k_4 &= f(Y(t_j) + h k_3, t_j + h, \beta_0, \beta_1). \end{aligned}$$

In the case of Equation (1) the time parameter t does not appear explicitly so our k formulas do not depend on it. We will refer to where the k parameters are estimated as 'sub-steps'. Note that t_j and $t_{j+1} = t_j + h$ are typically different to the times at which observations occur. The observation interval is an upper bound on the numerical step size h , but we can take multiple numerical steps between the observations.

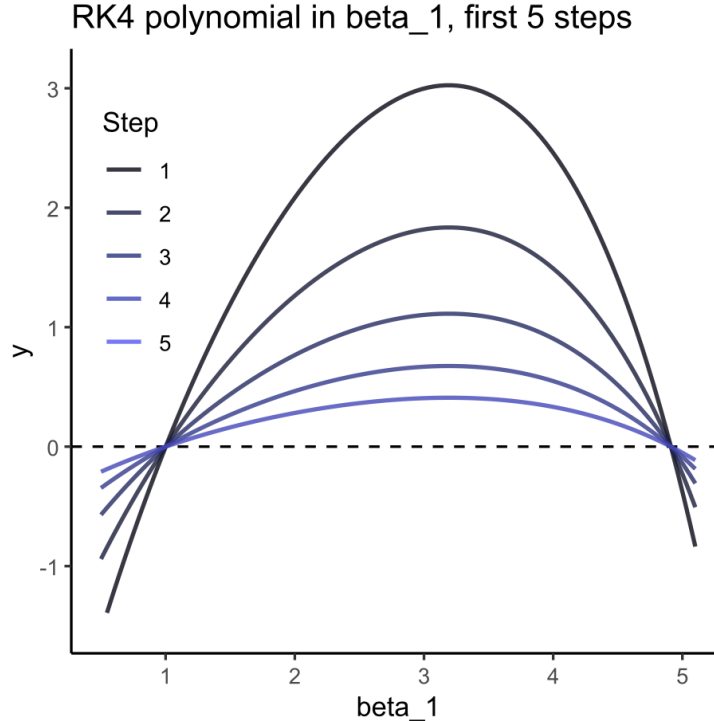


Figure 2: Plot of Equation (5) with $Y(t_j) = 1$ and $\alpha = 10$ for first five steps of size $h = 0.5$. The intersections with 0 are at $\hat{\beta}_1 = 1.0008$ and $\hat{\beta}_1 = 4.9112$.

It is precisely because the bad numerical method for $\beta_0 = 49.3$ and $\beta_1 = 4.91$ give $\hat{Y}(t_j)$ values so close to the analytic solution when $\beta_0 = 10$ and $\beta_1 = 1$ that we see the estimation problems. For a visual comparison see Figure 1(a) and (b). The estimation algorithm will converge to *any* parameter combination it finds that gives $\hat{Y}(t_j)$ close to the observations provided. In these cases the algorithm finds a point far from the true value where size estimates match the observations extremely well because of error in the numerical method. Non-identifiability here is not a problem with MCMC or another chosen estimation method, it is a structural issue arising from the use of numerical methods.

We can see the problem in plots of the estimated values for $Y(t)$ and $f(Y(t))$ at each step and sub-step for time from 0 to 4. Figure 1 shows instability of the numerical method at $\beta_0 = 49.3$, $\beta_1 = 4.91$, and stability at $\beta_0 = 10$, $\beta_1 = 1$. Both converge to the same asymptotic size $\beta_0/\beta_1 = 10$, but because we are using the numerical method to estimate longitudinal data, we care about the stability at the intermediate times as well. The main feature of interest is the huge variation of the \hat{Y} estimate in substeps given the erroneous parameter values, which comes from the gradient oscillating between positive and negative values in Panels (a) and (c). The excessive size happens when the increment estimate at a step $\hat{Y}(t_1)$ puts the next value $\hat{Y}(t_2)$ past the asymptotic limit β_0/β_1 , where the gradient is negative. Because the gradient at $\hat{Y}(t_2)$ is negative, the subsequent $\hat{Y}(t_3)$ value will be smaller. The numerical method at the pathological parameters is behaving so badly that we actually see a negative \hat{Y} value in the first integration's second substep.

In the case of Equation (1) we can leverage an explicit form of the RK4 algorithm in Equation (4) to get a polynomial in β_0 and β_1 ¹. We have to take care to differentiate the true parameters used in the analytic solution from the parameters we estimate from the longitudinal model, so we denote the estimated parameters with $\hat{\beta}_0$ and $\hat{\beta}_1$. For a step size of h , given initial size $Y(t_j)$ and the size at the next numerical step from the analytic solution $Y(t_j + h)$ we get

$$0 = Y(t_j) - Y(t_j + h) + h\hat{\beta}_0 - \hat{\beta}_1 \left(hY(t_j) + \frac{h^2}{2}\hat{\beta}_0 \right) + \hat{\beta}_1^2 \left(\frac{h^2}{2}Y(t_j) + \frac{h^3}{6}\hat{\beta}_0 \right) - \hat{\beta}_1^3 \left(\frac{h^3}{6}Y(t_j) + \frac{h^4}{24}\hat{\beta}_0 \right) + \hat{\beta}_1^4 \frac{h^4}{24}Y(t_j).$$

The affine DE with negative slope always converges to the asymptotic size $\hat{\beta}_0/\hat{\beta}_1 = \alpha$, and in fact if we make the substitution $\alpha\hat{\beta}_1 = \hat{\beta}_0$ we can refine further to get

$$0 = Y(t_j) - Y(t_j + h) + (\alpha - Y(t_j)) \left(h\hat{\beta}_1 - \frac{h^2}{2}\hat{\beta}_1^2 + \frac{h^3}{6}\hat{\beta}_1^3 - \frac{h^4}{24}\hat{\beta}_1^4 \right) \quad (5)$$

in which constants are $Y(t_j)$, $Y(t_j + h)$, t_j , h , and α . Given these values, the $\hat{\beta}_1$ solutions of Equation (5) will be the non-identifiable posterior modes. Through further work it may be possible to prove general non-identifiability for the von Bertalanffy model (affine first order ODE with negative slope) under RK4 with fixed step size. Such a proof is outside the scope of this thesis.

In our example case the asymptotic solution is $\hat{\beta}_0/\hat{\beta}_1 = 10 = \alpha$ (this is a very strong relationship in the data too), so we get

$$0 = Y(t_j) - Y(t_j + h) + (10 - Y(t_j)) \left(h\hat{\beta}_1 - \frac{h^2}{2}\hat{\beta}_1^2 + \frac{h^3}{6}\hat{\beta}_1^3 - \frac{h^4}{24}\hat{\beta}_1^4 \right).$$

In theory Equation (5) could be expanded to include all the time-steps, iterating through substitutions of $Y(t_j + 2h)$ and so on. Any values of $\hat{\beta}_1$ that solved the extended version of Equation (5) would be indistinguishable in the posterior. Such a calculation is outside the scope of this paper, but we can look at the solutions for each time step. We implemented Equation (5) in R and looked at the first five steps of $h = 0.5$ from Figure 1 to see if there are multiple zeroes. The results are in Figure 2 and show that each step has two solutions, and that those solutions are the same across the steps.

We can also do an explicit calculation for the first step with our estimated parameters. For our true values $\beta_0 = 10$, $\beta_1 = 1$ and $Y(t_j) = Y(0) = 1$, the analytic solution of the first step given $h = 1/2$ is $Y(0.5) = 4.541224$. Substitution of h , $Y(t_j)$, and $Y(t_j + h)$ into Equation (5) gives us a formula for the first step:

$$0 = 1 - 4.541224 + 9 \left(\frac{1}{2}\hat{\beta}_1 - \frac{1}{8}\hat{\beta}_1^2 + \frac{1}{48}\hat{\beta}_1^3 - \frac{1}{384}\hat{\beta}_1^4 \right). \quad (6)$$

The two solutions to Equation (6) are $\beta_1 = 1.0008$ and 4.9112 , which aligns with Figure 2 and what we observe in our posterior bimodality (allowing for numerical error and noise).

¹Computation in the supplementary material.

To show that this problem is not a quirk of our chosen parameter values, we consider Equation (5) for $\beta_0 = 8$, $\beta_1 = 1.5$, $Y(t_j) = 1$. The asymptotic size is $\beta_0/\beta_1 = \alpha = 16/3$, so we substitute in $\hat{\beta}_0 = \frac{16}{3}\hat{\beta}_1$ and get

$$0 = Y(t_j) - Y(t_j + h) + \frac{13}{3} \left(\frac{1}{2}\hat{\beta}_1 - \frac{1}{8}\hat{\beta}_1^2 + \frac{1}{48}\hat{\beta}_1^3 - \frac{1}{384}\hat{\beta}_1^4 \right). \quad (7)$$

The solutions to Equation (7) for $Y(t_j) = 1$ and $h = 0.5$ are $\hat{\beta}_1 = 1.5076$ and 4.5678 , and we have non-identifiability again.

Equation 5 is calculable directly because we have an analytic solution, explicit numerical method, and a straight-forward function. Attempts to do the same with the non-linear Canham function (Canham et al., 2004) for example would be impossible as there is no analytic solution for comparison. While the substitution with the analytic solution is not essential to testing a step where a better numerical method can give $Y(t_j + h)$, it would be intractable for Canham anyway due to the non-linear DE. In general it may not be possible to do an explicit formula of that form. Simulation is much easier and the user can test different methods and estimation tools as well.

2 Methods

We have three questions about the pathological behaviour, each of which required different testing.

- *Do different integration methods have persistent bimodality?* We have demonstrated mathematical bimodality for RK4 with a step size of 0.5 so we test whether that shows up empirically as well. We also do empirical tests for RK4 with step sizes 0.25 and 0.125, RK45 with adaptive step size, and an analytic solution.
- *Can changes to estimation method limit the impact of bimodality?* We test different prior configurations for MCMC using the RK4 method with a step size of 0.5, and also test a deterministic optimisation algorithm L-BFGS using the default priors.
- *Do our chosen solutions give unimodal, unbiased estimates?* We do simulation studies for the affine and Canham models to test whether the solutions implemented in `hmde` have reliable results.

The data we use is simulated so we know the true values. We produce ‘true’ data from the analytic solution Equation (3) with parameters $\beta_0 = 10$, $\beta_1 = 1$ and initial size $Y(0) = 1$. The simulated survey structure is 10 size values $Y(t_j)$ with an interval of 1 unit of time between them, so $t_{j+1} - t_j = 1$. From the analytic sizes over time we get ‘observations’ with error, rounded to precision 0.1, of the form

$$y_j = \text{round}(Y(t_j) + \mathcal{N}(0, 0.1), 0.1).$$

The simulation structure was chosen to behave like observations in centimetres with precision of 1 mm, and measurement error with 1 mm standard deviation. Results for the first two questions are based on running independent chains on the same set of 10 observations, so those results are

conditioned on a single dataset. Figure 4(a) shows the single simulated dataset in comparison to the analytic solution. To test whether the implemented solution to bimodality is robust we simulate observations independently for each chain based on the same underlying $Y(t_j)$.

For each test we ran 10,000 fits. In the case of MCMC this is 10,000 independent chains, while for the optimisation algorithm it is 10,000 runs each of which randomly selects a starting point in the parameter space. The large sample size was chosen because in initial testing we found that the second mode for the smallest RK4 step size was very rare and wanted to effectively estimate the mixture model probability.

Estimation of β_0 and β_1 employs a single-individual version of the hierarchical Bayesian longitudinal model introduced in O’Brien et al. (2024), with implementation and workflow based on `hmde` (<https://github.com/traitecoevo/hmde>). As there is only one individual, the model lacks a ‘population’ level, and instead we have fixed priors on the distributions for the two function parameters. Estimation is done through Markov Chain Monte Carlo sampling or a deterministic method (L-BFGS optimisation) implemented in Stan (Stan Development Team, 2022) via RStan (Stan Development Team, 2019). Code at <https://github.com/Tess-LaCoil/hmde-be-dragons> allows for complete reproduction of these results and further investigation as required.

The fixed step sizes (0.5, 0.25, 0.125) were chosen for both providing an integer number of sub-steps to the observation period $t_{j+1} - t_j = 1$, and because larger step sizes had bad numerical behaviour in the proximity of the true parameter values.

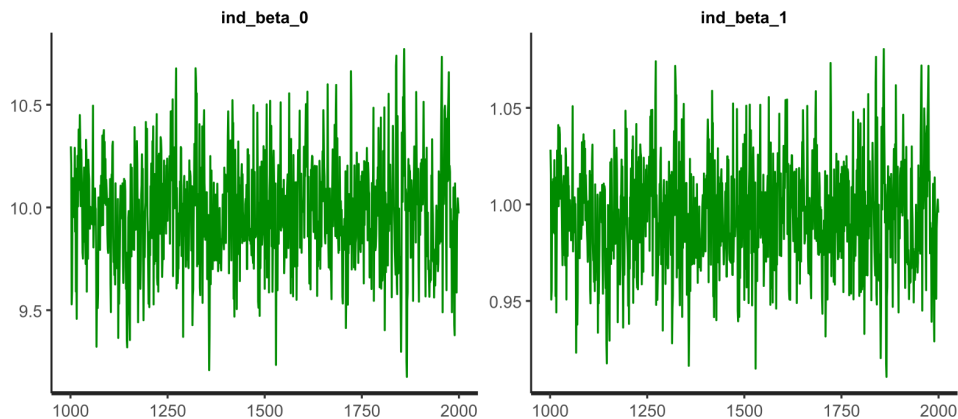
From each chain we extract the estimates $\hat{\beta}_0$ and $\hat{\beta}_1$ as the means of the posterior samples. We fit multivariate normal finite mixture models (McLachlan et al., 2019) to the 10,000 estimates for each MCMC model using the `mixtools` package (Benaglia et al., 2009). We can identify the posteriors that have two clusters through visual analysis of scatter plots as the clusters are very distant from each other, and the distance is much larger than the within-cluster variance with no values in the space between them. To initialise the finite mixture algorithm, we classify clusters by taking points on either side of the sample mean for $\hat{\beta}_0$, giving

$$g_1 = \{(\hat{\beta}_{0,j}, \hat{\beta}_{1,j}) : \hat{\beta}_{0,j} \leq \bar{\hat{\beta}}_0\}, \quad g_2 = \{(\hat{\beta}_{0,j}, \hat{\beta}_{1,j}) : \hat{\beta}_{0,j} > \bar{\hat{\beta}}_0\}.$$

We initialise the finite mixture algorithm with the sample means of the two groups to avoid convergence problems. The fitted mixture of normal distributions is then used to analyse the clustering behaviour, as we get cluster mean estimate vectors, covariance matrices, and cluster occurrence probability estimates. We also use scatter plots to look at the cluster marginal posterior parameter distributions. In the unimodal case we look at the mean of the estimated posterior parameters to understand bias, and a 95% posterior credible interval (Gelman et al., 2021) built from taking the central 95% quantile interval of the posterior estimates to get an idea of spread.

With the estimates in hand we can independently verify the numerical error using the `ode` function from the `deSolve` package (Karline Soetaert et al., 2010), which has its own implementation of the Runge-Kutta 4th order method (`rk4`). We plot the $Y(t_j)$ values for the true and estimated parameters with the step size used in the MCMC sampling and show that they are statistically indistinguishable by calculating the root mean squared error. We use plots of the analytic solutions

(a) Good est. traceplots: $\beta_0 = 9.97$, $\beta_1 = 0.994$



(b) Bad est. traceplots: $\beta_0 = 49.3$, $\beta_1 = 4.91$

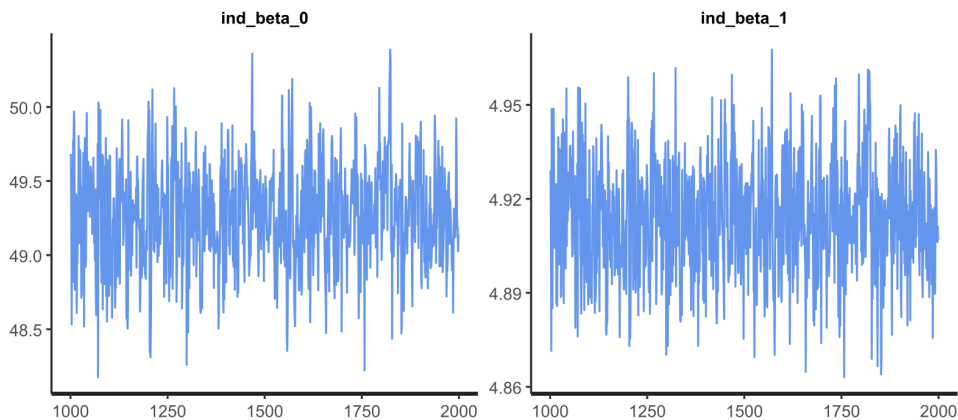


Figure 3: “Well-behaved” chains converging to very different estimates of the parameters $\beta_0 = 10$, $\beta_1 = 1$. (a) produced good estimates while (b) converged to the erroneous parameter combination.

to show that the erroneous parameter combinations actually produce very different behaviour in the absence of numerical error.

As we are running tens of thousands of simulations and looking for bad behaviour in the estimates we do not check diagnostics for every fit. In practice, consistent convergence of chains to different estimates is an indicator of posterior multi-modality and the numerical error may be a source of it. In Figure 3 we give examples of two chains fit with RK4 and a step size of 0.5 that appear to be well-behaved despite one of the two converging to the incorrect parameters, indicating that typical diagnostic plots alone may not be enough.

2.1 Checking Canham

We use simulation to check whether the Canham model used in `hmdc` is robust to posterior clustering due to numerical error with the RK45 method and adaptive step size. The differential equation

defined in [Canham et al. \(2004\)](#) is

$$f(Y(t), g_{max}, y_{max}, k) = g_{max} \exp \left(-\frac{1}{2} \left(\frac{\ln(Y(t)/y_{max})}{k} \right)^2 \right), \quad (8)$$

which is extremely non-linear and has no analytic solution, necessitating numerical methods within the longitudinal model. Equation (8) has advantages for numerical estimation over the affine ODE: it is strictly positive which helps avoid the extreme oscillation we see in [Figure 1](#) from negative growth, and it is bounded above by g_{max} which limits how big positive growth increments can get. The affine function is unbounded above and below, and as a negative growth increment can lead to negative $Y(t)$ values even if the data is strictly positive (Canham is undefined for $Y(t) \leq 0$ due to the log function), it is possible for the numerical method to encounter extreme positive growth increments as well as negative ones.

There is no analytic solution to Equation (8) which would give access to ‘true’ sizes over time $Y(t)$. Instead we used the `deSolve` RK4 method with step size 0.0001 to project forward 50 units of time from an initial size of $Y(0) = 1$. The true parameters $g_{max} = 0.8$, $y_{max} = 8$, $k = 1$ were chosen as plausible values based on what was observed in [O’Brien et al. \(2024\)](#). To test whether the step size was small enough to give good numerical estimates, we did the same forward projection with step size 0.001 and compared the two, which gave a maximum difference of 3.02×10^{-13} . We fit 10,000 chains to ‘observed’ sizes: from the smaller step size, we took 10 points, 5 years apart as the true values, then for each chain we add independent error from $\mathcal{N}(0, 0.1)$, and rounded to precision 0.1. The scale of error and measurement precision aligns with real-world data from [Condit et al. \(2019\)](#). We did not use the more faithful error model of [Rüger et al. \(2011\)](#) which is a mixture of normal distributions because [O’Brien et al. \(2024\)](#) found that doing so does not meaningfully change estimation. We add error independently for each chain as we are interested in whether the Canham model has bias as well as multimodality because it is the function and numerical method implemented in `hmde`.

For analysis we look at the posterior distribution of parameter estimates. Scatter plots and histograms are used to examine clustering. We use the mean of the estimates and central 95% posterior credible interval to examine spread and bias. The posterior is unimodal and attempts to fit a mixture distribution with two clusters failed as a result, so we do not use one.

3 Results

We see persistent bimodality across numerical methods with fixed step size. The location of the second mode depends on the numerical method. Changing the location of the parameter priors is unable to constrain the occurrence of the erroneous mode, while constraining the prior spread only eliminates the second mode when the standard deviation is too small to be of practical use. The methods implemented in `hmde` produce unbiased, unimodal estimates for both the affine and Canham models.

Table 1: Posterior finite mixture model estimates for MCMC testing different numerical methods. True parameter values are $\beta_0 = 10$ and $\beta_1 = 1$.

Numerical method	Step size	Cluster 1		Cluster 2		Cluster 2
		$\mu_{\beta_0,1}$	$\mu_{\beta_1,1}$	$\mu_{\beta_0,2}$	$\mu_{\beta_1,2}$	prob.
RK4 step size analysis	0.5	9.956	0.9917	49.26	4.913	0.3195
	0.25	9.949	0.991	104.5	10.47	0.1044
	0.125	9.949	0.9909	211.6	21.57	0.0254
RK45, $\beta_c \sim \mathcal{N}$	Adaptive	9.949	0.9909	9.949	0.9909	0.4729
RK45, $\beta_c \sim \log \mathcal{N}$	Adaptive	9.945	0.9906	10.19	1.015	0.80

3.1 Numerical methods have persistent bimodality

All the step sizes tested with the RK4 algorithm had a second cluster of erroneous parameter estimates. As the step size shrinks, the erroneous cluster moves further away from the true values, and the probability of erroneous convergence decreases as shown in Table 1. Figure 4 shows the cluster distance in Panel (b), where all 30,000 estimates are plotted together. There is a stack of points at (9.95, 0.991) which is the first cluster of estimates for all step sizes, and each step size has a second cluster spread further from that point as the step size decreases. The clusters all lie along a line preserving the asymptotic size at $\hat{\beta}_0/\hat{\beta}_1 \approx 10$, which is also visible in Figure 4(c) and (d). Panel (c) shows Equation (1) with parameters fit to the mean of each erroneous cluster compared to the true values, and Panel (d) shows the analytic solution Equation (3) with the same. The erroneous cluster has much faster analytic solution convergence to the asymptotic size, but as we saw in Figure 1, that leads to bad numerical behaviour.

For each step size we give more detailed plots. Figure 5(a), (c) and (e) show that the numerical estimates at the erroneous cluster strongly agree with the analytic solution for the true parameters, while (b), (d) and (f) shows how numerical error behaves badly by comparing the numerical estimates at the erroneous cluster to the analytic solution at the same parameter values.

Figure 6 gives a close-up view of the two clusters for each step size, and show that there is variation in the estimates at the small scale that is not visible in Figure 4(b). There is a strong relationship between the parameters that reflects the asymptotic size being tightly constrained by the observations at $\hat{\beta}_0/\hat{\beta}_1 \approx 10$.

We tested a better numerical method as well – RK45 with adaptive step size – and found that under some prior specifications bimodality still occurred. Figure 7 shows unimodal posteriors for both the analytic and RK45 posteriors when β_c has a normal prior, while Figure 8 shows the bimodal posterior that arose when we were testing a log-normal distribution for β_c with RK45, a problem that the analytic solution does not have. Log-normal priors are common so we include this example as a warning, even though the prior implemented in `hmde` does not demonstrate bimodality with

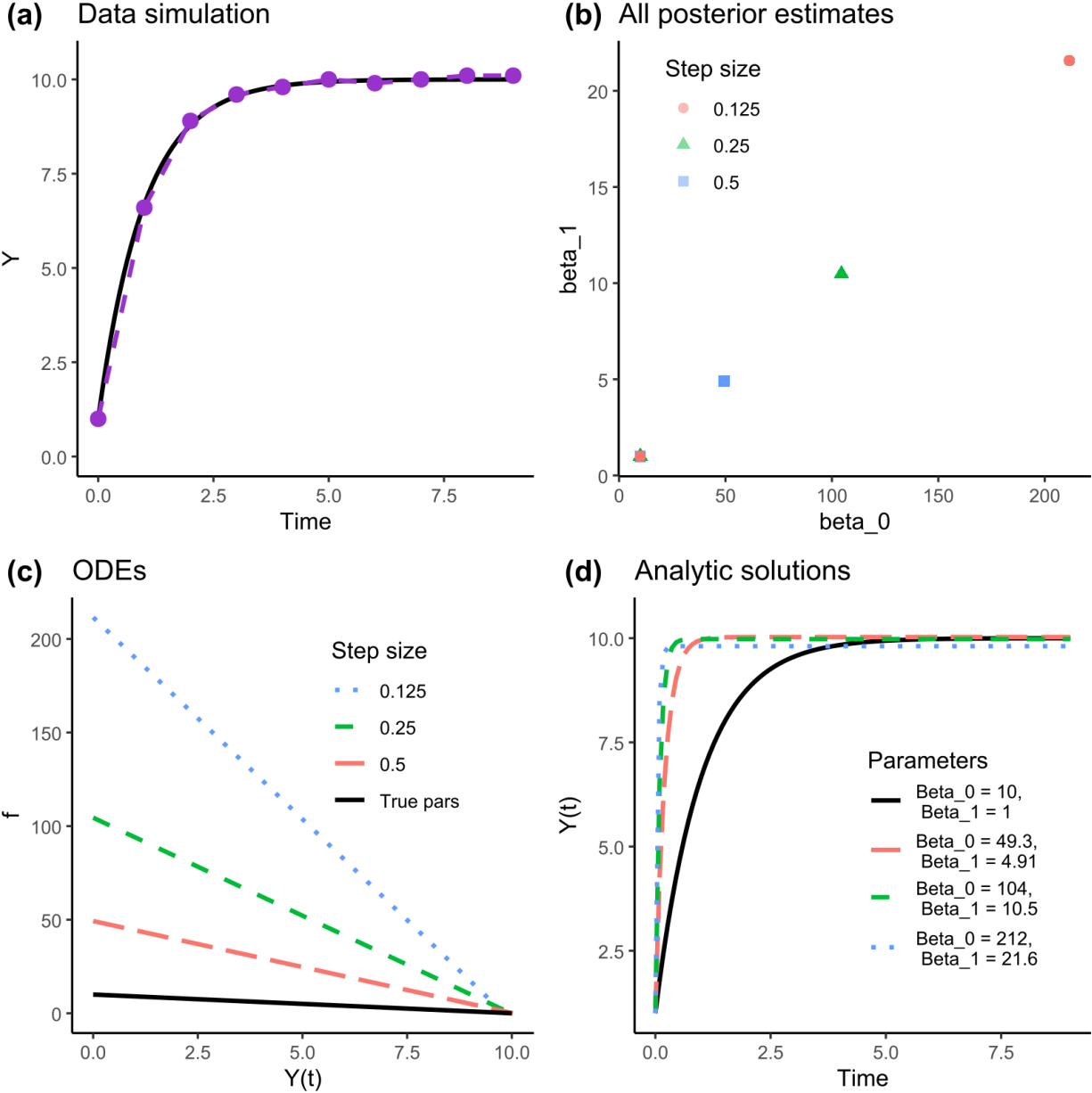


Figure 4: **(a)** gives the simulated data with measurement error and precision of 0.1 compared to the analytic solution for $\beta_0 = 10, \beta_1 = 1$. Outside of the specified situations with independent error for each chain, estimation is based on the same data. **(b)** is a scatter plot of all posterior estimates, good and bad, for the default priors across three step sizes using RK4. The ‘points’ are distributions of estimates. There is a stacked cluster for all step sizes at the true values, and each step size has a separate second cluster of erroneous values. **(c)** gives the erroneous differential equations and shows that all estimates converge to the same maximum size. **(d)** shows the analytic solutions using the erroneous parameter combinations to show that the erroneous values give sizes that converge to the asymptotic maximum much faster than the true solution.

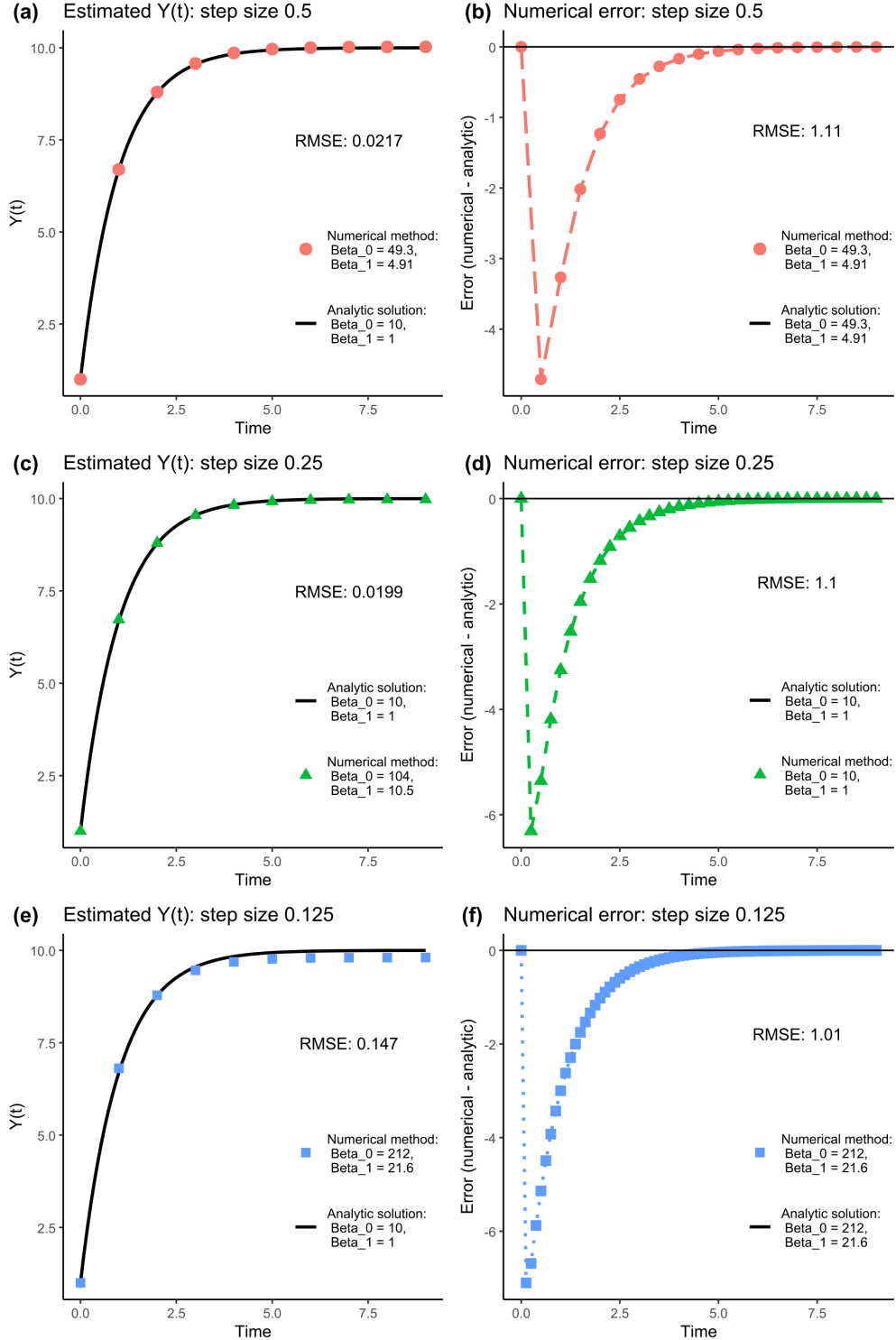


Figure 5: Estimated sizes over time across three step sizes compared to the true model for simulated data, and numerical error. (a), (c), and (e) show that the estimated sizes over time for the erroneous cluster align closely with the analytic solution for the true β s across the step sizes. The slight bias for step size 0.125 is likely due to the prior constraining $\hat{\beta}_0$. (b), (d), and (f) show the numerical error for each erroneous cluster, where the initial step has the largest error and then there is convergence to the same asymptotic size.

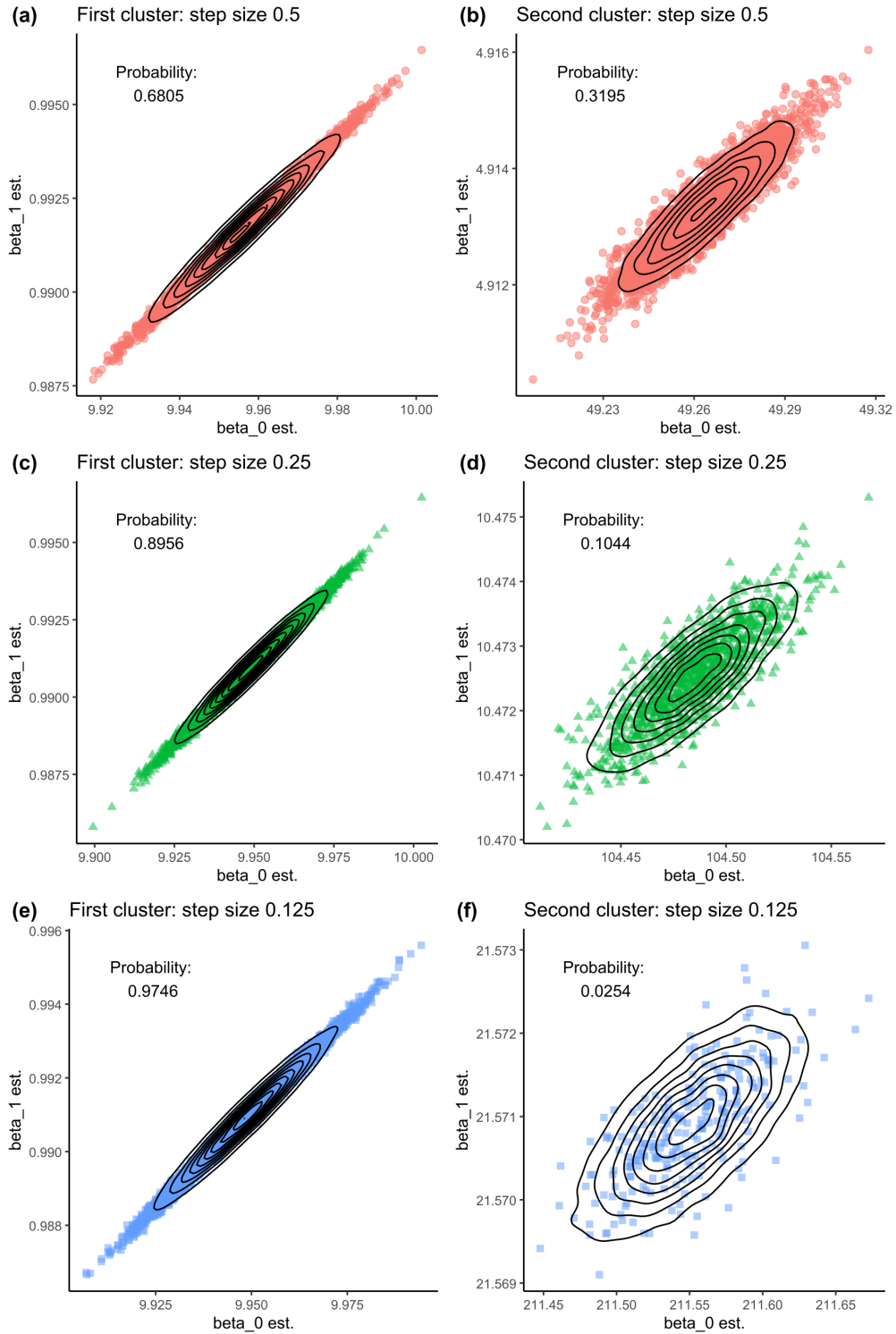


Figure 6: Posterior estimates scatter plots across three step sizes. (a) and (b) show clusters for step size 0.5. (c) and (d) show the clusters for step size 0.25, where the second cluster is further away from the first than for the larger step size and occurs less frequently. (e) and (f) show the first, and even more distant and less likely second cluster for the smallest step size 0.125.

RK45. Table 1 gives the mixture-model analysis for RK45. We do not consider the two clusters for $\beta_c \sim \log \mathcal{N}$ to be meaningfully different as they are so close together.

3.2 Changes to estimation methods do not address the underlying issue

Table 2 shows that all alternate priors except for one with an unreasonably small standard deviation picked up an erroneous second mode. The prior density is calculated after the fact by taking the product of normal distribution function values (as the two parameters are treated as independent in the prior) at the posterior cluster’s location using the prior parameters for mean and standard deviation. The density represents the height of the prior probability density function at that point. The posterior probability comes from the mixture distribution estimate.

Changing the prior central location had minimal impact, as can be seen in the first three prior configurations in Table 2. The ‘good’ modes had very similar locations, and the probability of converging to the second (erroneous) mode was not substantially different across the fits. The behaviour of the different centres is very similar the RK4 with 0.5 step size and default prior as seen in Table 1. That the posterior probability did not change even when the prior was centred at one or the other cluster indicates that changing the prior location does not help with constraining erroneous convergence.

A much larger prior standard deviation of 10 produced results that were not meaningfully different from the default of 2. Reducing the prior standard deviation to 0.1 changed where the second mode was, but did not meaningfully constrain its occurrence with a reduction from 32% to 26%. The even more unreasonably small prior standard deviation (0.001) was able to eliminate the second mode as the distance between the two means from the mixture model was vanishingly small. The purpose of including an unreasonable standard deviation prior was to demonstrate that it is mathematically possible to constrain where the posterior goes, but to do so requires something that would not be used in practice.

The deterministic algorithm L-BFGS performed badly overall, as seen in Figure 9. The figure represents 10,000 fits. There were problems where the randomly selected starting point failed to converge for a substantial region of the parameter space. Where the L-BFGS algorithm did converge, it had bimodal estimates.

3.3 Our chosen methods produce unbiased, unimodal estimates

The simulation tests for the affine model with an analytic solution produced a unimodal distribution that was centred within 0.3% of the true values as shown in Table 3. Using the analytic solution means we do not introduce the non-identifiability that arises from numerical error so this result is in line with our theory.

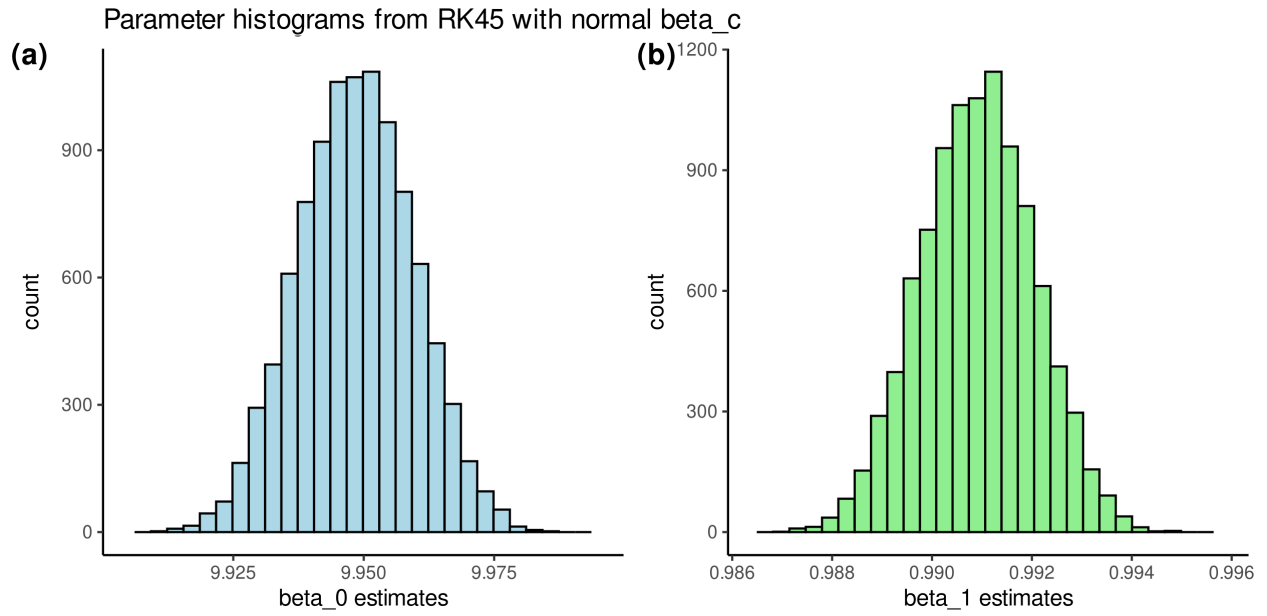


Figure 7: (a) and (b) show that the RK45 algorithm gives a unimodal posterior for both parameters when fit with a normal distribution prior on β_c .

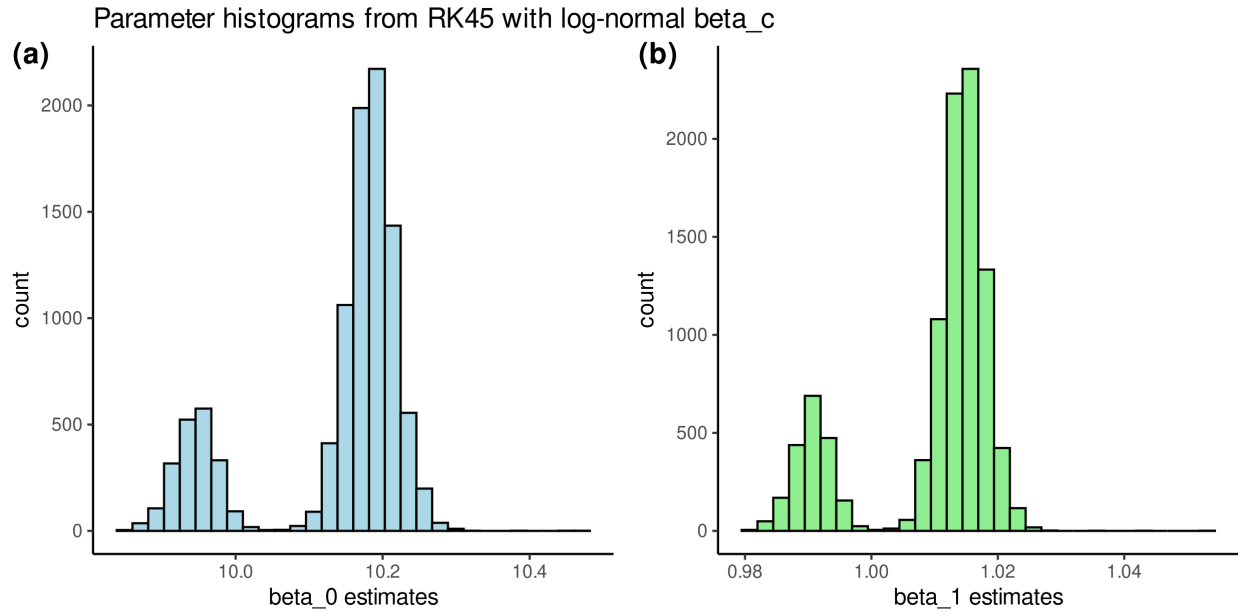


Figure 8: (a) and (b) show that bimodality can arise with the RK45 algorithm when β_c has a log-normal prior, and in fact the second mode is more likely than the first.

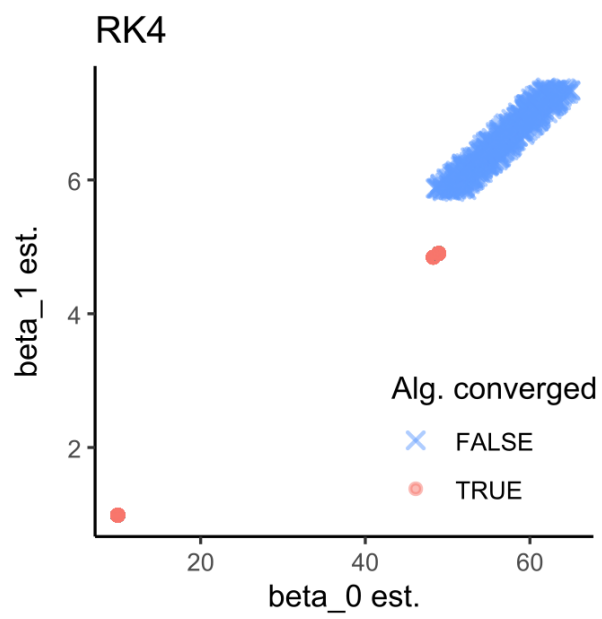


Figure 9: Estimation with L-BFGS optimisation algorithm. The deterministic method with the RK4 algorithm failed to converge in 5.8% of runs that randomly started in a pathological region as indicated by the blue crosses.

Table 2: Posterior finite mixture model estimates for MCMC with different priors. True parameter values are $\beta_0 = 10$ and $\beta_1 = 1$. The numerical integration was RK4 with a step size of 0.5. The β_c prior mean includes the \bar{y} shift, and the β_1 mean has a log transformation.

Priors	Posterior locations						Prior density		Posterior prob.		
	Cluster 1		Cluster 2		Cluster 1	Cluster 2	Cluster 1	Cluster 2	Cluster 1	Cluster 2	
	$\mu_{\beta_0,1}$	$\mu_{\beta_1,1}$	$\mu_{\beta_0,2}$	$\mu_{\beta_1,2}$							
Good estimate	$\beta_c \sim \mathcal{N}(1.43, 2)$										
centre	9.957	0.9918	49.27	4.914	0.03979	0.0005852	0.6871	0.3129	0.6871	0.3129	
Bad estimate	$\beta_c \sim \mathcal{N}(7.09, 2)$										
centre	9.969	0.9928	49.37	4.917	0.0005286	0.03979	0.6822	0.3178	0.6822	0.3178	
Midpoint	$\beta_c \sim \mathcal{N}(4.26, 2)$										
	$\beta_1 \sim \log \mathcal{N}(1.09, 2)$										
	9.963	0.9923	49.32	4.915	0.0126	0.01456	0.6805	0.3195	0.6805	0.3195	
Large SD	$\beta_c \sim \mathcal{N}(1, 10)$										
	$\beta_1 \sim \log \mathcal{N}(0, 10)$										
	9.957	0.9917	49.370	4.9170	1.590e-3	1.306e-3	0.6842	0.3158	0.6842	0.3158	
Small SD	$\beta_c \sim \mathcal{N}(1, 0.1)$										
	$\beta_1 \sim \log \mathcal{N}(0, 0.1)$										
	9.765	0.976	41.65	4.581	0.0153	1.085e-83	0.7437	0.2563	0.7437	0.2563	
Silly small	$\beta_c \sim \mathcal{N}(1, 0.001)$										
SD	$\beta_1 \sim \log \mathcal{N}(0, 0.001)$										
	9.599	0.9999	9.599	0.9999	149400	149400	0.4072	0.5928	0.4072	0.5928	

Table 3: The affine model with an analytic solution and the Canham model with RK45 and an adaptive step size show no evidence of bias.

Model	Parameter	True value	Mean est.	95% CI
Affine	β_0	10	10.02	(9.484, 10.57)
	β_1	1	1.002	(0.9445, 1.062)
	g_{max}	0.8	0.799	(0.776, 0.823)
Canham	y_{max}	8	7.979	(7.642, 8.301)
	k	1	1.009	(0.952, 1.073)

The overall behaviour of the posterior estimation for Canham is shown in Figure 10. We have a unimodal posterior distribution with no evidence of additional clusters in any dimension. Parameter estimation information is given in Table 3. We can be reasonably confident that the Canham function is not subject to the same pathologies as Equation (1) given the RK45 algorithm with adaptive step size used in the longitudinal model.

The associations between g_{max} and k , y_{max} and k in Figure 10(g) and (h) have an interpretation that works with the shape of the function in Panel (b): as k increases, if g_{max} decreases you will get similar total growth but more spread out over the observation period; and for k and y_{max} a negative relationship means that the hump will be more pronounced if y_{max} is large. We suspect that there is a connection between the sampling design (10 observations, 5 units of time apart) and how well the peak can be observed. Investigating that is outside the scope of this paper.

4 Discussion

This paper provides theoretical and empirical evidence of a bimodal posterior arising from numerical error in a longitudinal model for an affine first order ODE. One posterior mode aligns with good estimates of the true parameter values for simulated data, and at that mode the numerical method is reasonably well behaved. The other mode has extremely bad estimates of the true parameters, and badly behaved numerics as well. Theoretically, we show that in our chosen situation the RK4 numerical method has two parameter values that give the same sizes over time. In the empirical results, we see two clusters of parameter estimates that produce statistically indistinguishable $\hat{Y}(t_j)$. The empirical parameter estimates align closely with the theoretical results.

We demonstrated the bimodal posterior for Equation (1), and show that the behaviour can occur for different step sizes, priors, true parameters, numerical methods, and estimation methods. Where the second mode is located depends on the numerical method and step size, as which combination of bad parameters gives ‘correct’ $\hat{Y}(t_j)$ depends on both those factors. Changes to the prior distribution were unable to appropriately constrain the second mode, but implementing the analytic solution instead of using a numerical method eliminated the erroneous parameters in

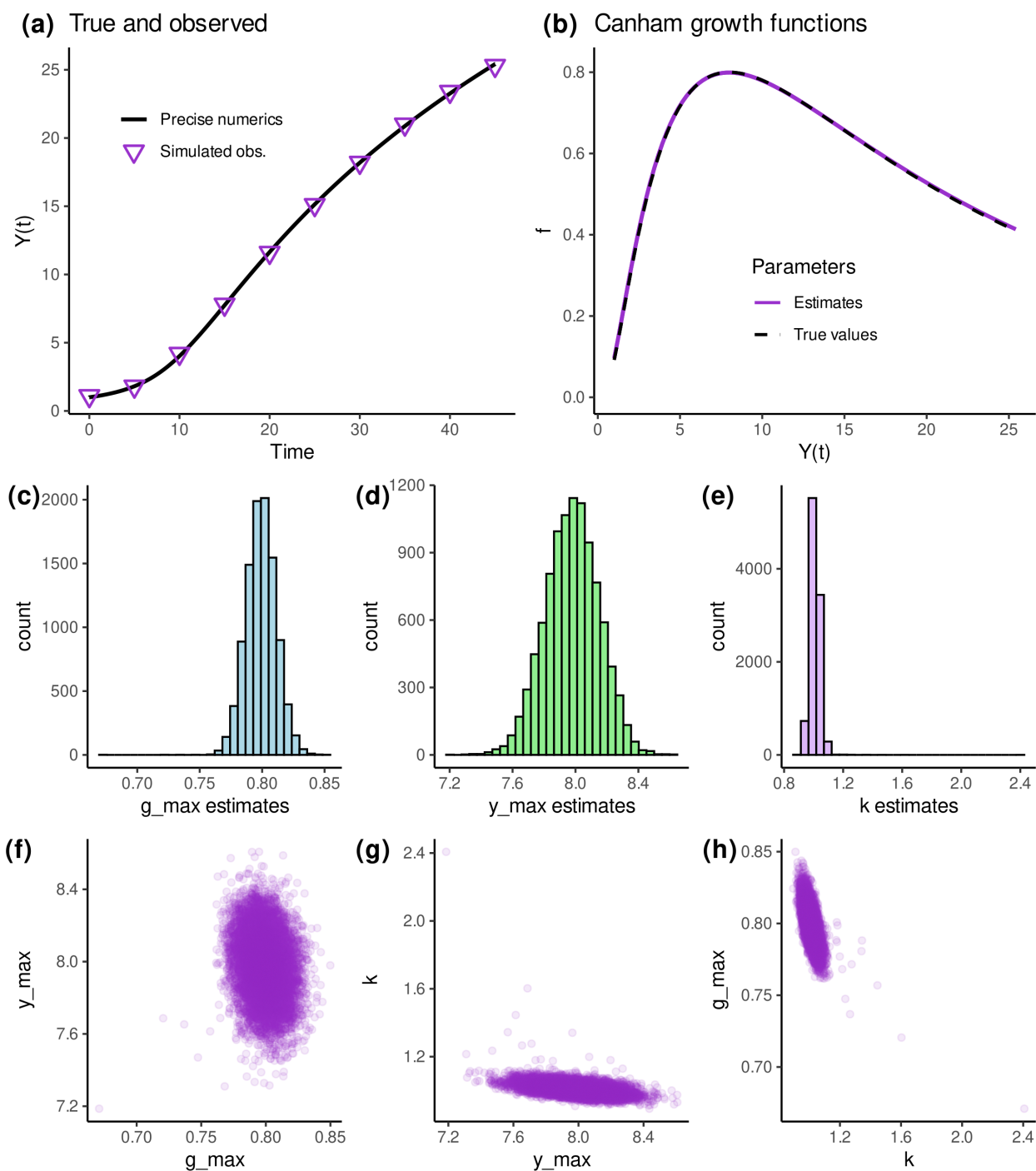


Figure 10: (a) shows an example of how the observations compare to the high precision numerical solution given $\mathcal{N}(0,0.1)$ error and measurement precision of 0.1. (b) compares the estimated and true growth functions which demonstrate strong agreement. (c), (d), and (e) histograms of the posterior parameter estimates demonstrate the unimodal posterior distribution and show no evidence of bi- or multi-modality. (c), (d), and (e) pair scatter plots of the posterior parameter estimates show no evidence of multi-modality, and moderate associations between g_{max} and k , y_{max} and k . The scatter plots and histograms are aligned on the horizontal parameter axis for ease of comparison.

MCMC sampling.

The persistence of bimodal posteriors due to numerical error indicate that choice of integration method matters beyond bias in estimating the posterior parameters. Bias has been tested in [Agapiou et al. \(2014\)](#) and [O’Brien et al. \(2024\)](#). The integration methods chosen to be implemented in the package `hmde` produced unimodal, unbiased estimates when tested in simulation for both the affine model where we used the analytic solution, and the second non-linear DE known as the Canham function ([Canham et al., 2004](#)) which under RK45 with an adaptive step size has unbiased, unimodal posteriors.

Our testing of different priors is distinct from the method recommended by [Gabry et al. \(2019\)](#). We seek to have default priors that resemble common choices to show that bimodality occurs, then test a specific set of priors to see if the problem can be averted. The choice of $\beta_1 \sim \log \mathcal{N}(0, 2)$ and $\beta_c \sim \mathcal{N}(1, 2)$ would likely be ‘vague’ under the taxonomy proposed by [Banner et al. \(2020\)](#), though the standard deviation of 2 is much smaller than some choices for flat priors. Instead, the default standard deviation represents what could be plausible given the magnitude of measurement (on the order of 1 to 10 cm) and the observed growth rates with a large-ish variance. The default priors are less important as we are not doing inference on data, we want to see if prior selection can constrain bimodality. We found that location did not and the prior standard deviation needed to be unreasonably small to eliminate the second mode, far smaller than would ever be used in practice. We do note that changing the prior distribution for the RK45 method from $\beta_c \sim \log \mathcal{N}(0, 2)$ to $\mathcal{N}(1, 2)$ did eliminate the second mode, so there may be specific cases where prior distribution choice works. The failure to eliminate the second mode with prior specification for the RK4 method is because the priors do not address the actual source of the problem.

Estimation methods are a consideration for models for both material (computation time) and theoretical reasons. We tested the computationally-intensive MCMC sampling method, and a computationally inexpensive but demonstrably less robust L-BFGS optimisation method that maximises the joint posterior likelihood. Neither avoided bimodality on their own because they too do not address the underlying numerical problems. MCMC sampling requires the numerical calculations to be run thousands of times so while an erroneous cluster can be identified after the fact with a high precision (and computationally expensive) numerical method, implementing that directly in the longitudinal model is not so feasible. That problems can be identified after the fact is helpful at least. In some cases multiple chains run in parallel can detect a bimodal posterior if they converge to different points, which is how we first observed the issue as tweaks to the von Bertalanffy model in `hmde` with RK4 failed to avoid the occasional chain converging to a secondary mode. Working with a small number of parallel chains is less reliable as a means of identifying posterior bimodality than large-scale simulation testing as we have done in this paper, particularly when the probability of converging to the second mode is small as for the affine model with step size 0.125.

If using empirical testing alone, MCMC may fail to detect numerical problems in parts of the parameter space, an issue pointed to by [Rannala \(2002\)](#) in a different context. If the user’s goal is to get a good estimate and not be waylaid by misbehaving numerics, that is a good thing. If the aim is to determine where numerical methods fail to work for the specified model, a more sensitive method

such as L-BFGS may be better for scoping out the posterior. There are alternate algorithms around, including in the inverse problem literature more broadly. [Bardsley et al. \(2014\)](#) uses a combination of random sampling and deterministic optimisation for example. Methods proposed by [Pompe et al. \(2020\)](#); [Syed et al. \(2022\)](#) and the annealed leap-point sampler (ALPS) ([Tawn et al., 2021](#); [Roberts et al., 2022](#)) are intended for multi-modal posteriors, but are not readily accessible to users. As the numerical integration is separate to the estimation structure, the suggestion in [Lele and Dennis \(2009\)](#) that frequentist likelihood maximisation methods may be preferred is not a solution for these situations.

The biggest consequence of bimodal non-identifiability in Bayesian inverse methods that use numerical integration is that even if a reasonable set of ‘true’ parameters is known, stability for the numerical methods matters for potentially a very large region of the parameter space. For the smallest step size we tried, the Euclidean distance between the good and bad modes was 217, and we found that constraining the priors did not meaningfully affect the posterior mode probability for the larger step size.

The numerical pathologies we found are adjacent to those addressed in the typical Bayesian workflow ([Gelman et al., 2020](#)), as the error comes from the longitudinal structure that is not part of most models. The simulation testing that we propose for posterior bimodality is relatively easy to implement, compared to hard-core numerical analysis for example, and can be done prior to large-scale dataset estimation. Aside from the affine model, we applied simulation tests to the extremely non-linear Equation (8), where we cannot apply an analytic solution to avoid bimodality as there isn’t one. In the case of the Canham function we are able to test for evidence of a bimodal posterior and parameter bias under the implemented numerical method – RK45 with adaptive step size – and find none. As a result we can be confident that the implementation of the Canham model in `hmdc` is unlikely to be as problematic as the von Bertalanffy model was without the analytic solution.

We have shown that simulation can detect bimodality, but even a unimodal posterior should be checked with a better numerical method after sampling. If the numerical method in the model behaves badly at the estimated parameters, the estimates cannot be trusted. In a more general setting, when using models that rely on numerical methods, numerical error should be considered alongside other sources such as measurement error ([Cotter et al., 2010](#)).

Non-identifiability arising from numerical error in a longitudinal model does not appear to be addressed elsewhere in the identifiability literature. More attention is paid to situations where the data is insufficient to uniquely specify estimates from a theoretical standpoint, whether due to too large a parameter space for the observations ([Gelfand and Sahu, 1999](#)) or large measurement uncertainty ([Auger-Méthé et al., 2016](#)). [Gelman et al. \(2020\)](#) Section 11 addresses multi-modality that arises from orbit periodicity where there are not enough observations to select a specific value. Our problem arises in the model, but the literature around model structure tends to focus on over-parameterisation ([Rannala, 2002](#)), or prior specification ([Gelfand and Sahu, 1999](#)), neither of which are the problem here. As such, we hope this case study can expand the known issues with identifiability in inverse problems and Bayesian methods, and provide answers for someone else who has gotten stuck on a similar issue.

5 Conclusions

Here we document the discovery and investigation of a novel source of non-identifiability in Bayesian inverse methods. We have shown that posterior bimodality can arise from an interaction between numerical integration error in a longitudinal model and MCMC sampling of integrand parameters.

For a known troublemaker ODE – Equation (1) – posterior bimodality was persistent across three step sizes for RK4, different priors, estimation methods, and true parameters. Only an analytic solution implemented in the longitudinal model was able to correct the issue. For a more numerically amenable function – Equation (8) – we have no evidence of bimodality with an RK45 method using adaptive step size, and demonstrate successful testing of numerical pathologies through simulation.

As Bayesian inverse methods develop, knowing where and how numerical error can introduce pathologies is essential to good estimation. We have demonstrated one such problem and solution, in a manner that is hopefully useful elsewhere.

References

- Agapiou, S., Bardsley, J. M., Papaspiliopoulos, O., and Stuart, A. M. (2014). Analysis of the gibbs sampler for hierarchical inverse problems. *SIAM/ASA Journal on Uncertainty Quantification*, 2(1):511–544.
- Auger-Méthé, M., Field, C., Albertsen, C. M., Derocher, A. E., Lewis, M. A., Jonsen, I. D., and Mills Flemming, J. (2016). State-space models’ dirty little secrets: even simple linear gaussian models can have estimation problems. *Scientific reports*, 6(1):26677.
- Banner, K. M., Irvine, K. M., and Rodhouse, T. J. (2020). The use of bayesian priors in ecology: The good, the bad and the not great. *Methods in Ecology and Evolution*, 11(8):882–889.
- Bardsley, J. M., Solonen, A., Haario, H., and Laine, M. (2014). Randomize-then-optimize: A method for sampling from posterior distributions in nonlinear inverse problems. *SIAM Journal on Scientific Computing*, 36(4):A1895–A1910.
- Benaglia, T., Chauveau, D., Hunter, D. R., and Young, D. (2009). mixtools: An R package for analyzing finite mixture models. *Journal of Statistical Software*, 32(6):1–29.
- Butcher, J. C. (2016). *Numerical methods for ordinary differential equations*. John Wiley & Sons, third edition.
- Canham, C. D., LePage, P. T., and Coates, K. D. (2004). A neighborhood analysis of canopy tree competition: effects of shading versus crowding. *Canadian Journal of Forest Research*, 34(4):778–787.
- Cockayne, J., Oates, C. J., Sullivan, T. J., and Girolami, M. (2019). Bayesian probabilistic numerical methods. *SIAM review*, 61(4):756–789.
- Condit, R. (1998). *Tropical forest census plots: methods and results from Barro Colorado Island, Panama and a comparison with other plots*. Springer Science & Business Media.
- Condit, R., Pérez, R., Aguilar, S., Lao, S., Foster, R., and Hubbell, S. (2019). Complete data from the barro colorado 50-ha plot: 423617 trees, 35 years, 2019 version.
- Cotter, S. L., Dashti, M., and Stuart, A. M. (2010). Approximation of bayesian inverse problems for pdes. *SIAM journal on numerical analysis*, 48(1):322–345.
- Falster, D. S., Brännström, Å., Westoby, M., and Dieckmann, U. (2017). Multitrait successional forest dynamics enable diverse competitive coexistence. *Proceedings of the National Academy of Sciences*, 114(13):E2719–E2728.
- Gabry, J., Simpson, D., Vehtari, A., Betancourt, M., and Gelman, A. (2019). Visualization in bayesian workflow. *Journal of the Royal Statistical Society Series A: Statistics in Society*, 182(2):389–402.

- Gelfand, A. E. and Sahu, S. K. (1999). Identifiability, improper priors, and gibbs sampling for generalized linear models. *Journal of the American Statistical Association*, 94(445):247–253.
- Gelman, A., Carlin, J. B., Stern, H. S., and Rubin, D. B. (2021). *Bayesian data analysis*. CRC Press, 3rd april 2021 edition.
- Gelman, A., Vehtari, A., Simpson, D., Margossian, C. C., Carpenter, B., Yao, Y., Kennedy, L., Gabry, J., Bürkner, P.-C., and Modrák, M. (2020). Bayesian workflow. *arXiv preprint arXiv:2011.01808*.
- Iida, Y., Kohyama, T. S., Swenson, N. G., Su, S.-H., Chen, C.-T., Chiang, J.-M., and Sun, I.-F. (2014). Linking functional traits and demographic rates in a subtropical tree community: the importance of size dependency. *Journal of Ecology*, 102(3):641–650.
- Karline Soetaert, Thomas Petzoldt, and R. Woodrow Setzer (2010). Solving differential equations in R: Package deSolve. *Journal of Statistical Software*, 33(9):1–25.
- Latz, J. (2023). Bayesian inverse problems are usually well-posed. *SIAM Review*, 65(3):831–865.
- Lele, S. R. and Dennis, B. (2009). Bayesian methods for hierarchical models: are ecologists making a faustian bargain? *Ecological applications*, 19(3):581–584.
- McLachlan, G. J., Lee, S. X., and Rathnayake, S. I. (2019). Finite mixture models. *Annual review of statistics and its application*, 6(1):355–378.
- Modrák, M., Moon, A. H., Kim, S., Bürkner, P., Huurre, N., Faltejsková, K., Gelman, A., and Vehtari, A. (2023). Simulation-based calibration checking for bayesian computation: The choice of test quantities shapes sensitivity. *Bayesian Analysis*, 1(1):1–28.
- Nocedal, J. and Wright, S. J. (2006). *Numerical Optimization*. Springer, 2nd ed. edition.
- O’Brien, T., Warton, D., and Falster, D. (2024). Yes, they’re all individuals: Hierarchical models for repeat survey data improve estimates of tree growth and sie. *Methods in Ecology and Evolution*, 16(1).
- O’Brien, T. A., Kar, F., Warton, D., and Falster, D. S. (2025). hmde: Hierarchical methods for differential equations. *bioRxiv*.
- Pompe, E., Holmes, C., and Łatuszyński, K. (2020). A framework for adaptive mcmc targeting multimodal distributions. *The Annals of Statistics*, 48(5):2930–2952.
- Rannala, B. (2002). Identifiability of parameters in mcmc bayesian inference of phylogeny. *Systematic biology*, 51(5):754–760.
- Roberts, G. O., Rosenthal, J. S., and Tawn, N. G. (2022). Skew brownian motion and complexity of the alps algorithm. *Journal of Applied Probability*, 59(3):777–796.

- Rothenberg, T. J. (1971). Identification in parametric models. *Econometrica: Journal of the Econometric Society*, pages 577–591.
- Rüger, N., Berger, U., Hubbell, S. P., Vieilledent, G., and Condit, R. (2011). Growth strategies of tropical tree species: disentangling light and size effects. *PloS one*, 6(9):e25330.
- Stan Development Team (2019). RStan: the R interface to Stan. R package version 2.19.2.
- Stan Development Team (2022). Stan Modeling Language Users Guide and Reference Manual. Version 2.33.
- Syed, S., Bouchard-Côté, A., Deligiannidis, G., and Doucet, A. (2022). Non-reversible parallel tempering: a scalable highly parallel mcmc scheme. *Journal of the Royal Statistical Society Series B: Statistical Methodology*, 84(2):321–350.
- Talts, S., Betancourt, M., Simpson, D., Vehtari, A., and Gelman, A. (2020). Validating bayesian inference algorithms with simulation-based calibration.
- Tawn, N. G., Moores, M. T., and Roberts, G. O. (2021). Annealed leap-point sampler for multi-modal target distributions. *arXiv preprint arXiv:2112.12908*.
- Von Bertalanffy, L. (1938). A quantitative theory of organic growth (inquiries on growth laws. ii). *Human biology*, 10(2):181–213.

Here Be Dragons: Supplementary material

Tess O'Brien, Matt Moores, David Warton, & Daniel Falster

February 18, 2025

1 Numerical calculations

The Runge-Kutta scheme for $Y(t)$ given $\frac{dY}{dt} = f(Y(t), t, \theta)$ is calculated as

$$Y(t_{j+1}) = Y(t_j) + \frac{h}{6}(k_1 + 2k_2 + 2k_3 + k_4) \quad (1)$$

where h is the step size and k values are estimates of the gradient at iterated points given by

$$\begin{aligned} k_1 &= f(Y(t_j), t_j, \theta), \\ k_2 &= f(Y(t_j) + hk_1/2, t_j + h/2, \theta), \\ k_3 &= f(Y(t_j) + hk_2/2, t_j + h/2, \theta), \\ k_4 &= f(Y(t_j) + hk_3, t_j + h, \theta). \end{aligned}$$

The affine model is

$$f(Y(t), \beta_0, \beta_1) = \beta_0 - \beta_1 Y(t), \quad (2)$$

which is time-independent so t does not appear. The following computations give us a polynomial in β_0 and β_1 . First we calculate formulas for each k_i that depend only on β s and $Y(t_j)$ by substituting in the function definition sequentially. First

$$k_1 = \beta_0 - \beta_1 Y(t_j),$$

which we substitute into k_2 to get

$$\begin{aligned} k_2 &= \beta_0 - \beta_1 \left(Y(t_j) + \frac{h}{2} k_1 \right) \\ &= \beta_0 - \beta_1 \left(Y(t_j) + \frac{h}{2} (\beta_0 - \beta_1 Y(t_j)) \right) \\ &= \beta_0 - \beta_1 \left(Y(t_j) + \frac{h}{2} \beta_0 \right) + \beta_1^2 \frac{h}{2} Y(t_j). \end{aligned}$$

Subsequent k s are

$$\begin{aligned}
k_3 &= \beta_0 - \beta_1 \left(Y(t_j) + \frac{h}{2} \beta_0 \right) + \beta_1^2 \left(\frac{h}{2} Y(t_j) + \frac{h^2}{4} \beta_0 \right) - \beta_1^3 \frac{h^2}{4} Y(t_j), \\
k_4 &= \beta_0 - \beta_1 (Y(t_j) + h\beta_0) + \beta_1^2 \left(hY(t_j) + \frac{h^2}{2} \beta_0 \right) \\
&\quad - \beta_1^3 \left(\frac{h^2}{2} Y(t_j) + \frac{h^3}{4} \beta_0 \right) + \beta_1^4 \frac{h^4}{4} Y(t_j).
\end{aligned}$$

To extract the polynomial we substitute the k s into Equation 1 and subtract $Y(t_{j+1})$ from both sides to get

$$\begin{aligned}
0 &= Y(t_j) - Y(t_{j+1}) + \frac{h}{6} \left[6\beta_0 - \beta_1(6Y(t_j) + 3h\beta_0) + \beta_1^2 \left(3hY(t_j) + h^2\beta_0 \right) \right. \\
&\quad \left. - \beta_1^3 \left(h^2Y(t_j) + \frac{h^3}{4}\beta_0 \right) + \beta_1^4 \frac{h^3}{4} Y(t_j) \right] \\
&= Y(t_j) - Y(t_{j+1}) + h\beta_0 - \beta_1 \left(hY(t_j) + \frac{h^2}{2}\beta_0 \right) + \beta_1^2 \left(\frac{h^2}{2} Y(t_j) + \frac{h^3}{6}\beta_0 \right) \\
&\quad - \beta_1^3 \left(\frac{h^3}{6} Y(t_j) + \frac{h^4}{24}\beta_0 \right) + \beta_1^4 \frac{h^4}{24} Y(t_j). \tag{3}
\end{aligned}$$

We can use the β_0 and β_1 solutions of Equation (3) to determine estimated parameters given we have an analytic solution to give us values for $Y(t_j)$ and $Y(t_{j+1})$.

References